DOI: 10.1021/ma102291m

Macromolecules
ARTICLE

Bioinspired Fibers Follow the Track of Natural Spider Silk

M. Elices,[†] G. V. Guinea,[†] G. R. Plaza,[†] C. Karatzas,[‡,§] C. Riekel,[∥] F. Agulló-Rueda,[⊥] R. Daza,[†] and J. Pérez-Rigueiro*,[†]

[†]*Departamento de Ciencia de Materiales, ETSI Caminos, Canales y Puertos, Universidad Politécnica de Madrid, 28040 Madrid, Spain,* [‡]*Nexia Biotechnologies Inc., Vaudreuil-Dorion, QC J7V 8P5Canada,* [∥]*European Synchroton Radiation Facility, B.P. 220, F-38043, Grenoble Cedex, France, and* [⊥]*Instituto de Ciencia de Materiales de Madrid, CSIC, Cantoblanco, 28049 Madrid, Spain.* [§]*Present address: The Research Institute of the McGill University Health Centre, Montreal, H3H 2R9, Canada*

Received October 7, 2010; Revised Manuscript Received January 11, 2011

ABSTRACT: The mechanical behavior and microstructure of bioinspired fibers spun from solutions of recombinant spidroin-like proteins were extensively characterized, and compared with those of natural spider silk fibers. It is confirmed that high performance bioinspired fibers indistinguishable from natural spider silk up to large strains can be produced through genetic engineering and conventional spinning technologies. It is also found that fibers spun from spidroin-like proteins that contain different motifs of sequence exhibit variations in their microstructure in terms of crystallinity and chain alignment, but these differences are not reflected in distinct tensile properties. This similarity in terms of their mechanical behavior indicates that bioinspired fibers are largely independent of their exact sequence of recombinant proteins and, in particular, of their proline content. Finally, it is shown that the largest differences between natural and bioinspired fibers are found at very large deformations, marking the ultimate challenge in the synthesis of silk-like fibers.

Introduction

Is it possible to synthesize bioinspired fibers that reach the outstanding properties of natural spider silk from genetically engineered protein solutions through an artificial spinning process? The answer to this simple question represents one of the most important challenges in the field of biomimetics, and its ultimate solution will largely influence the future development of the discipline.

The singular mechanical properties of silk fibers—namely, their unbeatable toughness[1] and their capability to recover from irreversible strains[2]—have placed them as one of the paradigms of natural structural materials[3] and have driven the quest for the development of synthetic counterparts in the past decade. The increasing knowledge gathered about composition, microstructure and processing of natural fibers has allowed significant progresses in the field, but bioinspired fibers still fall behind natural silks.

Production of artificial silk fibers requires the completion of two steps: (1) the synthesis of proteins and (2) the development of a spinning process that converts the protein solution into solid fibers, each of which represents a formidable technological problem.

Many initial attempts were essentially devoted to the use of recombinant biotechnology for the production of silk-like proteins. Although very few silk genes have been completely cloned[4,5] due to the large size of the silk proteins (≈300 kDa),[6] the existence of a small number of simple motifs of sequence extensively repeated[7] has led to the synthesis of artificial analogues, that are believed to capture the essential features of the natural proteins. The expression of these analogues has proceeded successfully in a number of different organisms such as bacteria,[8,9] yeasts,[10,11] plants,[12] and animal cells.[13,14]

Simultaneously, a different approach tried to establish the experimental conditions that led to the production of solid fibers from protein solutions.[15] Most studies used silkworm silk fibroin solutions due to the accessibility to large amounts of this protein compared with those obtained from other sources, leading to the so-called regenerated silk fibroin fibers (RSF). All spinning processes share a basic scheme based on the wet spinning technique,[16] in which the proteins solidify in a coagulation bath, so that different procedures differed in the composition of the initial protein solution (dope) and in the coagulation bath.[17−20]

The first attempt to obtain artificial fibers from a solution of recombinant proteins were reported by the DuPont group[21] using hexafluoro-2-propanol as solvent and spinning through a stainless steel spinneret into a coagulating bath of 2-propanol. However, it is usually accepted that the basic breakthrough in the field was the production of fibers with acceptable tensile properties by Nexia[13] using a solution of spidroin-like proteins (ADF-3, MW = 60 kDa) in phosphate-buffered saline and a methanol−water coagulating bath. Later attempts have tried to incorporate part of the complexity observed in the silk glands of arthropods, through the inclusion of processes such as salting out, pH drop and elongational flow during the spinning process[22] or with the use of microfluidic devices.[15]

However, despite these painstaking efforts, it can be considered that only a very limited success has been achieved in the production of regenerated and bioinspired silks, a situation that cast doubts on the overall adequacy of the artificial synthesis routes. In particular, it was not possible to discriminate between composition and processing conditions as the main target to act on in order to improve the characteristics of the bioinspired fibers.

In this work, we present the first comprehensive report on bioinspired fibers spun from a solution of recombinant spidroin-like proteins that yield tensile properties up to its breaking indistinguishable from those of the natural silks. The study extends to four groups of fibers produced from dopes of varying ratios of recombinant spidroin-1 and spidroin-2 (dragline spider silk) spun under the same wet-spinning processing conditions. The recombinant proteins are based on two polypeptides that

*Corresponding author.

 Published on Web 02/04/2011

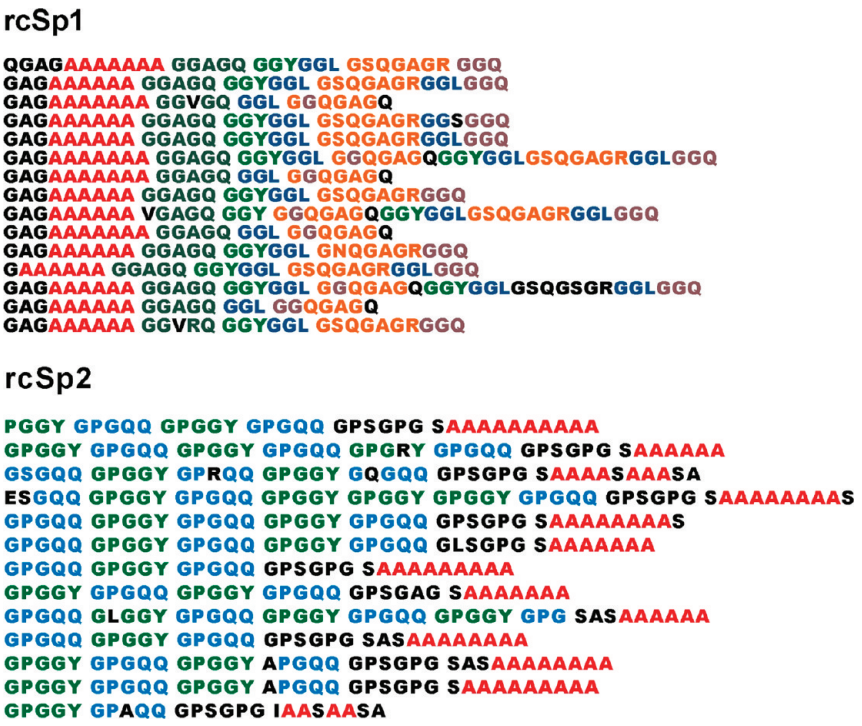

Figure 1. Complete sequences of the recombinant proteins rcSp1 and rcSp2 used in this work. Each sequence corresponds to a single molecule that contains the monomers ordered as indicated in the figure. The motifs of sequence are highlighted in different colors. rcSp2 contains the amino acid proline in the motif GPGQQ.

mimic different sequences of the spidroin-1 and spidroin-2[6] produced in the major ampullate gland of the spider *Nephila clavipes*. The results of the present study show that all compositions led to fibers with good mechanical properties (recoverability[2] and high toughness) irrespective of their sequence. The availability of these high performance fibers based on various ratios of recombinant spidroin-1 and -2 facilitates the study of which properties shown by the natural materials are relatively easy to regain in the artificial fibers and which will require additional developments.

Materials and Methods

Recombinant Silk Fibers Production. Two polypeptides have been used, that include the repetitive motifs of sequence of the major ampullate silk proteins of the spider *N. clavipes*,[7] including the carboxy-terminus. The polypeptides were labeled as rcSp1 and rcSp2 referring to the spidroin by which they are inspired, spidroin-1 (MaSp1) and spidroin-2 (MaSp2),[6] respectively. Their sequences are shown in Figure 1.

The production of the recombinant proteins, preparation of the spin dopes and spinning of the fibers is described in detail elsewhere.[13,23] The rcSp1 and rcSp2 proteins were purified to homogeneity from the milk of transgenic goats using a combination of tangential flow filtration and chromatography followed by alcohol precipitation and stored as dried powders. Purity of proteins as assessed by HPLC and SDS-PAGE followed by silver staining was >95%. Spin dopes were prepared by adding the desired volume of hexafluoro-2-propanol (HFIP) solvent to a weighed amount of powder protein in a glass vial (2−6 mL), which was then mounted on a vortex mixer and shaken until dissolved. Four dopes were prepared with different proportions by weight of the two recombinant proteins: 100−0, 70−30, 30−70, 0−100 (%rcSp1−%rcSp2).

A prototype melt extrusion spinning apparatus with extruder, two draw godets, heater, and winder was used (SpinLine, DACA Instruments, Goleta California) and converted to wet spinning apparatus suitable for the recombinant silk fibers production. The extruder barrel was modified such that syringes (Hamilton Gastight 1 or 2.5 mL with 1/4−28 "C" thread) could be inserted in order to load the extruder with small volumes of spin dope more easily. A 2-propanol coagulant bath, take-up roller, draw baths, steam source for fiber postspinning drawing were used for wet spinning of the fibers. Post treatment of the fiber was achieved by additional drawing, combined with heat treatment in steam for 5 min with a draw rate of 5-fold. All the fibers used in this work were processed under the same conditions.

Mechanical Tests. The fibers were tensile tested to measure the mechanical properties. Each sample was glued on a frame made of aluminum foil, as described elsewhere.[24] The gauge length, i.e., the length of the sample between the glued ends, was 25 mm. The frame was mounted in an Instron 4411 testing machine, and subsequently the aluminum frame was cut so that the entire load was transmitted through the fiber. The force was measured with an electronic balance (Precisa XT 220; resolution 0.1 mgf) placed under the lower grip. The displacement of the crosshead was taken as a direct measurement of the deformation of the fiber due to the large compliance of the fiber compared with the rest of the experimental setup. The validity of this assumption was checked on some selected samples by measuring the deformation on the fiber with an optical extensometer (Keyence LS-7500).

Tensile tests of the as spun fibers were performed either in air at 25 °C and 35% relative humidity or immersed in water.[25] Maximum supercontracted samples (see discussion on supercontraction below) were obtained following the same procedure used with major ampullate silk.[26] Briefly, the as spun sample was immersed in water and allowed to contract freely. Water was removed after 24 h and the fiber was dried overnight. Before testing, it was checked that the fiber remained slack after supercontraction, and tests proceeded in air at 25 °C and 35% relative humidity. The speed of the crosshead was fixed for all tests (as spun in air, as spun in water and supercontracted) at 1 mm/min.

Cross Section Measurements. In order to obtain the cross-section of the samples, two 5 mm long pieces, adjacent to both

sides of each sample were retrieved, metallized with gold, and observed in a scanning electron microscope (SEM-JEOL 6300; observation conditions $V = 10$ kV, $I = 0{,}6$ nA). At least four micrographs were taken from each sample. Diameters at a given section of the fiber were calculated as the average of at least 10 measurements on each micrograph, and the cross-sectional area was determined assuming a circular cross-section.

The cross-sectional areas were used to compute true stress-true strain curves, from force-displacement data. The cross-sectional area of the supercontracted fiber was calculated assuming that volume was conserved during supercontraction.[27]

X-ray diffraction. The fiber microstructure, crystallinity, and orientation distribution of crystalline domains were explored by synchrotron radiation raster microdiffraction using an $\approx 2 \times 2\ \mu m^2$ monochromatic beam at a wavelength of $\lambda = 0.0996$ nm.[28] Raster-diffraction scans were performed at 100 K with a step-resolution of 3 μm across and 5 μm along about 50 μm fiber sections. A CCD detector with 2K $\times$ 2K pixels and 16 bit readout was used for data collection with a typical exposure time of 2 s/pattern. The Q-range of $0.63 < Q\ (nm^{-1}) < 0.16$ provided moderate small-angle X-ray scattering (SAXS) resolution corresponding to a maximum d-spacing of $d_{max} = 2\pi/Q \sim 10$ nm. For background correction of the raster-scan data, scattering measured outside the fiber was subtracted using the FIT2D program.[29] Further details can be found in the Supporting Information.

Raman analysis. To measure the molecular alignment with respect to the fiber axis (z direction), polarized Raman spectra were collected with both the incident and scattered light either parallel (I_{zz}) or perpendicular (I_{xx}) to the fiber axis. A near-infrared (NIR) diode laser (Toptica dfBeam 785-S with optical isolator) was used for excitation to reduce fluorescence emission from the sample. Polarization direction was rotated with a zero-order precision quartz $\lambda/2$ wave plate. Laser light was focused on the fiber with a 100$\times$ Mitutoyo Plan NIR infinity-corrected microscope objective. Laser power on the sample was kept below 20 mW. At this power, the spectra did not change with time, avoiding any laser-induced damage. Each sample was analyzed at several points to check for possible inhomogeneities. Scattered light was collected with the same objective and analyzed with a 300 mm-focal-length single-grating spectrometer (Princeton Acton Spectra Pro 2300i) and a back-illuminated deep-depletion CCD detector (Princeton Pixis 256), thermoelectrically cooled (-75 °C) to reduce dark counts. Elastically scattered light was blocked with a long-wave pass edge filter (Semrock Razor Edge U grade). Polarization of the scattered light was selected by rotating a zero-order precision quartz $\lambda/2$ wave plate before a fixed dichroic glass linear polarizer. A 600-grooves/mm diffraction grating was used to measure the spectral range between 200 and 1900 cm^{-1} at once. A 1200-grooves/mm grating was used to measure the 1200$-$1700 cm^{-1} range with better spectral resolution. This range was chosen because it contains the amide III and amide I bands. They arise, respectively, from vibrations approximately parallel and perpendicular to the polypeptide backbone and their intensity in polarized spectra is very sensitive to the degree of orientation of the β-sheets.[30]

Atomic Force Microscopy. The nanostructural organization of the fibers was studied by means of atomic force microscopy. The details of the procedure have been described elsewhere.[31] Briefly, fibers were embedded in Spurr's resin and allowed to cure for 72 h at 70 °C. The function of the Spurr's resin is to serve as mechanical support to the fiber during the ultramicrotomy step. The longitudinal sections were obtained by ultramicrotomy with a diamond blade. The atomic force microscopy images were obtained in a Bermad 2000 AFM (Nanotec Electrónica, Spain), using Olympus OMCL RC800PSA cantilevers, and the highest resolution was obtained with the stiffest tip (nominal stiffness 0.76 N/m). AFM images were recorded in the dynamic mode in the repulsive regime of the tip$-$sample interaction.[32] The processing of the AFM images, consisting of simple equalizing and adjusting the contrast and the brightness of the micrographs, has been performed with the WSxM program (Nanotec, Spain).[33] No filter has been used to improve the quality of the images or to highlight their details.

Results and Discussion

1. Mechanical Properties of As Spun (AS) Recombinant Silk Fibers. The mechanical properties of recombinant silk fibers of the four compositions in the as spun condition are presented in Figure 2a, and their basic tensile parameters in Table 1. True stress$-$true strain curves were calculated from the measured diameters assuming the conservation of volume during the test.[27] All samples showed a very homogeneous cross section along their length. The range of curves obtained from naturally spun spider silk (i.e., MAS silk spun for building the web or as a safety line) as presented previously[34] is displayed in gray as a reference. It can be observed that all recombinant silk fibers display remarkable properties, with a tensile strength between 280 and 350 MPa, and elongation at break between 0.3 and 0.4. The tensile strength is still lower than the tensile strength of natural spider silk fibers, while the elongation at break approximately lies in the range of the values displayed by natural spider silk fibers.[34] Despite differences in composition it is found that the properties of the four types of fibers largely concur and, most significantly, are essentially indistinguishable from the natural material except for the lower value of tensile strength. From these results it is apparent that the differences in composition do not exert a significant influence on the mechanical properties of as spun recombinant fibers when tested in air.

2. Supercontraction and Recovery of Recombinant Fibers. Supercontraction is a singular property characteristic of major ampullate silk gland (MAS) fibers,[35,36] which is supposed to be linked with the outstanding performance of the material.[37] Supercontraction was identified and labeled from a significant reduction, up to a 60% of its initial value, in the length of unrestrained fibers when they are immersed in water or in highly humid environments.[38] This reduction is accompanied by a drastic change in the tensile properties of the fibers which, when tested in water, show the low initial stiffness and high strain at breaking of elastomers.[39] Besides, supercontraction seems to be characteristic of spider silk fibers, since it has not been found in silks from other species, such as silkworm silk.[1]

Although it was not acknowledged immediately, one of the deepest consequences of supercontraction is that it reflects the existence of a ground state in MAS fibers.[26] This ground state, usually labeled as maximum supercontracted (MS) state, can be recovered independently from the loading history of the material by simply subjecting the unrestrained fiber to water immersion and subsequent drying.[2] It has also been found that the whole range of tensile properties exhibited by MAS silk fibers including, but not restricted to, naturally spun fibers can be obtained in a reproducible way by simply stretching the fibers in water from the MS state and drying[40] (or conversely by limiting the amount to which the fiber is allowed to supercontract[26,41]). The discovery of the link between supercontraction in spider silk and the existence of the ground state has suggested a slight change in the terminology. Thus, the term supercontraction was proposed to be associated with the existence of a ground state independently of the exact value of the dimensional variation of the fiber induced by water immersion.[42]

The assessment of the existence of supercontraction in bioinspired fibers has important implications for the practical

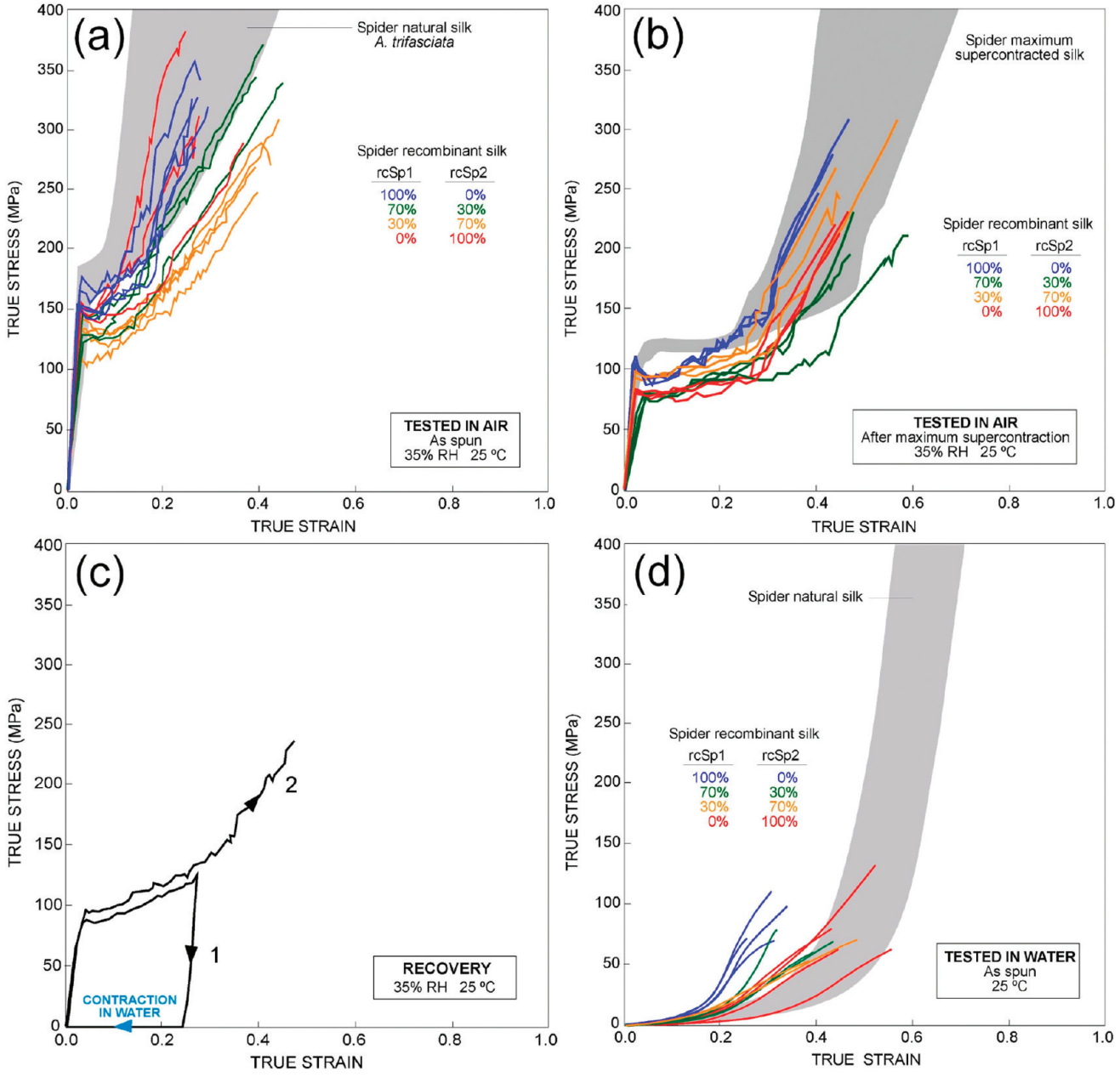

Figure 2. (a). True stress−true strain curves of as spun bioinspired fibers of the four compositions analyzed. The shaded area corresponds to the range of tensile properties exhibited by naturally spun fibers, i.e., as structural elements in the web or as a safety line, produced by *Argiope trifasciata* spiders as shown previously in ref 34. (b) True stress−true strain curves of maximum supercontracted bioinspired fibers of the four compositions analyzed. The shaded area corresponds to the range of tensile properties of maximum supercontracted fibers exhibited by spiders of the *Araneoidea* lineage as shown in Elices et al.[45] (c) Recovery test of a 70%−30% (rcSp1−rcSp2) fiber. Recovery tests consist of stretching a previously supercontracted fiber up to a given strain (0.25 in this figure), unloading (marked with a 1) and subjecting the fiber to a second maximum supercontraction process. The true stress-true strain curve of the fiber after supercontraction (marked with a 2) concurs with the initial curve, showing the ability of the fiber to recover from irreversible deformations. (d) True stress-true strain curves of bioinspired fibers of the four compositions tensile tested in water. The shaded area corresponds to the range of tensile properties of spider silk fibers tested in water exhibited by spiders of the *Araneoidea* lineage.

usage of the fibers due to the desirable properties, such as recovery and adaptability, imparted to the fiber. Of even deeper consequence is the singularity of supercontraction of MAS fibers, and its study in the artificial material offers the possibility of evaluating how close the present techniques allow reproducing the properties of the natural material. This rationale was reinforced by the discovery of supercontraction and recovery in regenerated silkworm silk fibers,[42] despite the fact that natural silkworm silk fibers do not show a similar effect. In effect, it has been found that silkworm silk show a small contraction (*Antheraea pernyi*, 5%;[43] *Bombyx mori*, 3%[25]), but contracted silkworm fibers neither show an elastomeric behavior[44] nor represent a ground state to which the fiber can revert.

The extent of supercontraction in recombinant fibers has been analyzed by measuring the reduction in length of unrestrained fibers in two steps: (1) measurement of the reduction in length after immersion in water and (2) measurement of the reduction in length after subsequent drying. The results expressed as the percentage of supercontraction (% SC = $100 \times (L_0 - L_{MS})/L_0$), where L_0 is the initial length of the fiber and L_{MS} is the length after supercontraction) are shown in Table 2. The data are the result of at least three different tests with each material. It can be observed that all

Table 1. Diameter and Tensile Parameters of the As Spun Recombinant Fibers[a]

(%rcSp1−%rcSp2)	D (μm)	E (GPa)	σ_y (MPa)	σ_u (MPa)	ε_u	W_f (MJ/m^3)
100−0	44 ± 3	7.7 ± 0.3	157 ± 6	320 ± 10	0.27 ± 0.00	55 ± 3
70−30	46 ± 2	6.3 ± 0.2	136 ± 4	350 ± 10	0.42 ± 0.02	70 ± 10
30−70	40 ± 3	5.6 ± 0.2	131 ± 5	280 ± 15	0.41 ± 0.01	72 ± 5
0−100	36 ± 2	7.4 ± 0.2	148 ± 3	330 ± 20	0.30 ± 0.05	62 ± 7
			N. inaurata Major Ampullate Silk (Forcibly Silked)			
	5.9 ± 0.2	14.2 ± 0.6	380 ± 10	1800 ± 60	0.26 ± 0.01	260 ± 5
			Ultrahigh Molecular Weight (UHMW) Polyethylene Fibers—Spectra 1000			
	27	175		3000	0.027	50
			Kevlar 49			
	12	125		2800	0.028	50

[a] Standard values of Spectra 1000 and Kevlar 49 are shown for comparison (E, elastic modulus; σ_y, yield stress; σ_u, ultimate tensile stress; ε_u, strain at breaking; W_f, work to fracture).

Table 2. Percentage of Supercontraction and Tensile Parameters of the Maximum Supercontracted Fibers[a]

(%rcSp1−%rcSp2)	% SC (% SC in water)	E (GPa)	σ_y (MPa)	σ_u (MPa)	ε_u	W_f (MJ/m^3)
100−0	17 ± 1 (3 ± 1)	5.9 ± 0.3	98.0 ± 1.3	280 ± 20	0.44 ± 0.02	75 ± 10
70−30	24 ± 1 (5 ± 2)	2.5 ± 0.3	80.8 ± 0.8	210 ± 10	0.52 ± 0.04	58 ± 4
30−70	16 ± 2 (6 ± 2)	4.9 ± 0.2	99.0 ± 0.6	270 ± 20	0.49 ± 0.04	69 ± 8
0−100	21 ± 4 (10 ± 3)	4.1 ± 0.1	82.0 ± 1.3	220 ± 5	0.45 ± 0.01	61 ± 8
			N. inaurata Major Ampullate Silk (Maximum Supercontracted)			
	41 ± 1	4.4 ± 0.4	203 ± 2	1460 ± 90	0.70 ± 0.02	270 ± 20

[a] The corresponding values of *N. inaurata* MAS fibers are shown for comparison (E, elastic modulus; σ_y, yield stress; σ_u, ultimate tensile stress; ε_u, strain at breaking; W_f, work to fracture).

materials show a relatively modest supercontraction in water, which increases significantly after drying. As was indicated by the tensile properties of the fibers in the as spun condition, there is not a clear correlation between the percentage of supercontraction and the composition of the fibers. The significant difference between the contraction observed during immersion and that measured after subsequent drying is also shown by other fibers processed artificially, such as regenerated silkworm silk fibers, and it has been explained in terms of the swelling of the fibers in water.[25]

The tensile properties of maximum supercontracted (MS) fibers tested in air are shown in Figure 2b and their tensile parameters presented in Table 2. The range of tensile properties of natural spider silk fibers spun by orb-web spinning spiders in the MS condition is represented by the shadowed area. This range was obtained from the stress−strain curves of MS fibers of six different orb web spinning species.[45] As it was observed with the fibers in the as spun condition, MS fibers show comparable tensile properties essentially independent of their exact composition and are indistinguishable from natural silk fibers except for the lower value of the tensile strength. This coincidence is even more striking than that observed between as spun and naturally spun fibers, since it shows the identity between the ground states of both bioinspired and natural materials.

It was finally assessed that supercontraction reflects the existence of a ground state in recombinant fibers and, consequently, the possibility of recovery from irreversible deformations. At least two recovery tests were performed for each recombinant fiber and it was found that these silks showed a ground state as illustrated in Figure 2c. Recovery tests proceeded by stretching a previously maximum supercontracted fiber in air up to a given deformation (25% in the test of Figure 2c). The fiber is then subjected to a second supercontraction step, dried and tensile tested until breaking. As is shown in Figure 2c the stress−strain curve of the stretched fiber after the second supercontraction step concurs with the original curve, substantiating that recombinant fibers do recover from irreversible deformations. Consequently, the effect of water on recombinant silk fibers can be identified properly as supercontraction.

In this regard, the results presented above cast light in the debate of the importance of the proline content in the supercontraction process. It has been found that proline content appears to influence significantly the supercontraction and the mechanical properties of natural spider silk produced by orb-web weaving spiders,[46] and the effect has been explained in terms of metastable order around proline groups.[47] However, the analysis of spider silk of nonorb-web weaving spiders that do not contain proline in its sequence[48] indicate that, albeit it seems to exert a significant influence in the extent of supercontraction, proline residues are not necessary for spider silk to supercontract. The results presented above support this view since all four compositions (two containing proline, two depleted of proline residues) show comparable values of length variation by supercontraction and a ground state.

3. Mechanical Properties of Recombinant Silk Fibers in Water. Supercontraction can be considered probably as the most singular of the effects that water exerts on the tensile properties of spider silk, since it was found that water modifies considerably the overall mechanical properties of the fibers. This influence can be essentially traced back to a change in the glassy-rubbery transition of spider silk, which is dependent on both temperature and relative humidity.[38,49] The effect of water on the glass transition of spider silk was explained at a molecular level as the result of eliminating the hydrogen bonds between protein chains, so that the tensile properties are controlled by the elastomeric behavior of the chains.[42] This elastomeric behavior is measured when the spider silk fibers are tested in water.[39]

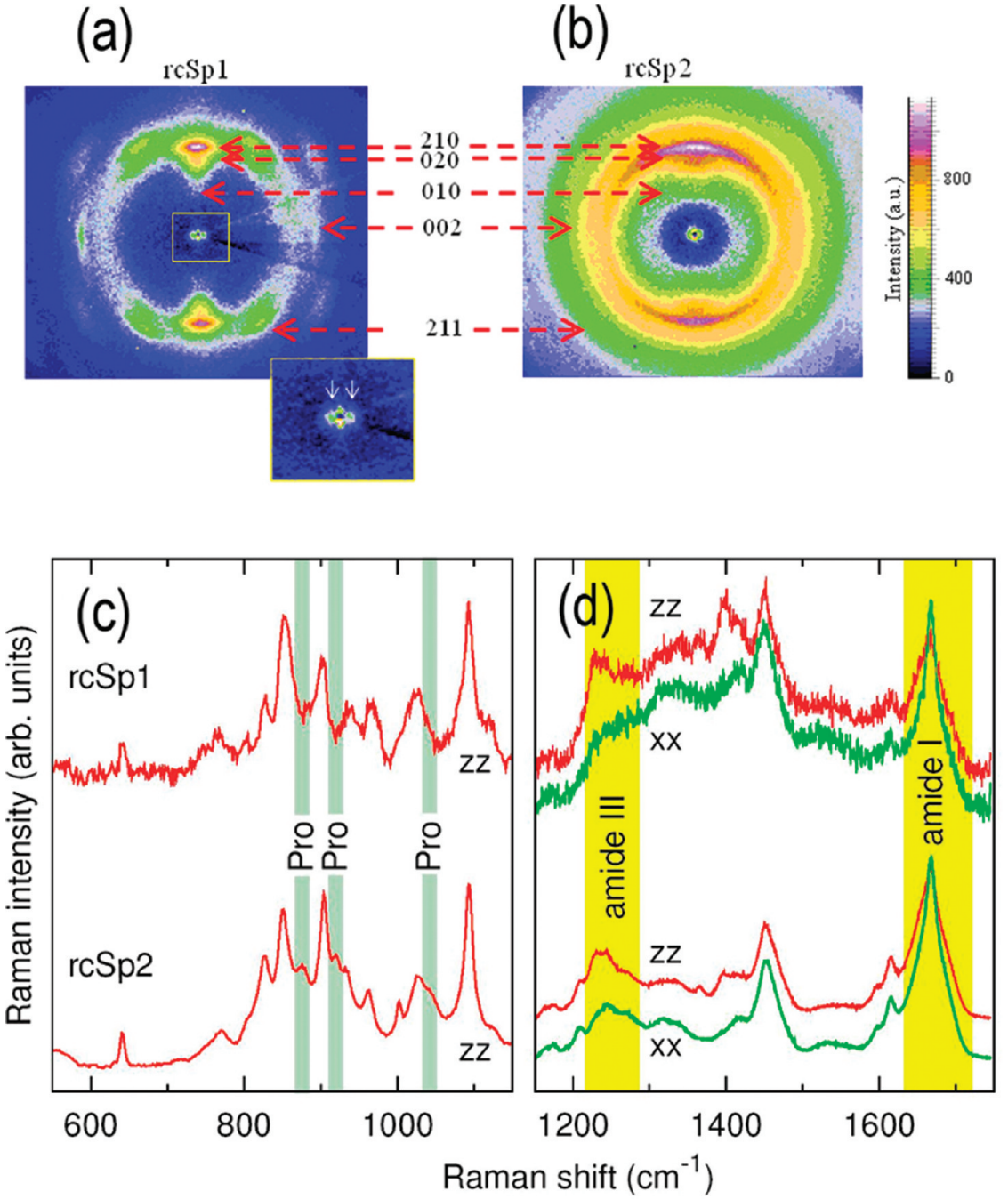

Figure 3. X-ray diffraction patterns of (a) pure rcSp1 (100%−0%) and (b) pure rcSp2 (0%−100%) fibers. The fiber axis lies in the horizontal direction. The inset shows a zoom of the rcSp1 pattern and reveals the SAXS range in more detail. The white arrows indicate the meridional SAXS peak. (c and d) Raman spectra of pure rcSp1 (100%−0%) and pure rcSp2 (0%−100%) fibers measured with a 785 nm-wavelength laser. Incident and scattered light polarization directions (*xx* or *zz*) are indicated (*z* is taken parallel to the fiber axis). Spectra have been vertically offset for clarity. (c) Vertical bars indicate the position of peaks characteristic of proline (P) and show differences in the amino acid composition of the two fibers. (d) Polarization anisotropy of the amide III and amide I peaks (position indicated by vertical bars).

Figure 2d shows the true stress−true strain curves of the recombinant silk fibers tested in water. The shadowed region corresponds to the range of stress−strain curves of natural spider silk fibers as obtained from the comparison of MAS silk from six different orb-web spinning spiders.[45] The elongation at breaking (0.35−0.55) and especially the tensile strength (50−150 MPa) of recombinant silk fibers are significantly lower than those of natural silk fibers. In contrast to the tensile properties of recombinant fibers in air, it was observed that their mechanical properties in water were distinctly dependent on the composition. The rcSp1 (100%−0%) fibers showed an overall stiffness greater than that of the rcSp2 (0%−100%). rcSp2 tested in water are indistinguishable from their natural counterparts except for their lower tensile strength.

Thus, although water exerts a plasticizing effect for all compositions, this effect increases with the proline content.

4. X-ray Diffraction. X-ray diffraction shows that rcSp1 (100%−0%) and rcSp2 (0%−100%) fibers are homogeneous materials on the micrometer-scale without skin/core morphologies. The rcSp1 and rcSp2 diffraction patterns correspond to the β-poly(L-alanine) structure of spider MAS silk[50] which has been structurally first described in refs 51 and 52 (Figure 3a,3b; Table 3). Both patterns show a

mixture of Bragg peaks due to nanocrystalline domains and short-range order scattering from the amorphous protein matrix. Details of the analysis of the patterns in terms of crystallinity, particle size and molecular orientation are provided in the Supporting Information. The size of the nanocrystalline domains of 2−3 nm in rcSp1 and rcSp2 corresponds to that of MAS-silk.[50,53] The crystallinity of natural MAS silk of ∼12%[54] is situated between that of rcSp1 silk (∼18%) and rcSp2 silk (∼10%). The higher crystalline volume fraction and hence lower short-range order volume fraction of rcSp1 silk is also reflected by a higher crystalline domain orientation distribution as compared to rcSp2 silk.

Table 3. Crystal Structure, Crystallinity, and Molecular Order (in Terms of Azimuthal Width of the 210/020 Planes) of Recombinant Silk Fibers

sample	structure	crystallinity (%)	orientation distribution (fwhm, deg)
rcSp1	β-poly(L-alanine)	18	210: 19.5 020: 19.5
rcSp2	β-poly(L-alanine)	10	210: 32.6 020: 30.5

A meridional SAXS peak with $d \sim 7.4$ nm for rcSp1 silk (inset in Figure 3a) is also observed in natural MAS silk from *Nephila* spiders.[55,56] The peak in natural MAS silk has been attributed to alanine-rich nanocrystalline domains, capped on both sides by glycine-rich short-range order domains, which assemble into nanofibrils of ∼165 nm.[56] The observation of a single SAXS peak in natural MAS silk and rcSp1 suggests only a weak density correlation. It is not excluded that the rcSp2 protein assembles according to the same scheme as rcSp1. The lower poly(alanine) content of the rcSp2 protein implies, however, a weaker scattering contrast, and the lower orientation distribution a more diffuse distribution so that the SAXS peak could be too weak to be observable.

5. Micro-Raman Spectra. Parts c and d of Figure 3 show the polarized Raman spectra of the rcSp1 (100%−0%) and rcSp2 (0%−100%) fibers. The region between 500 and

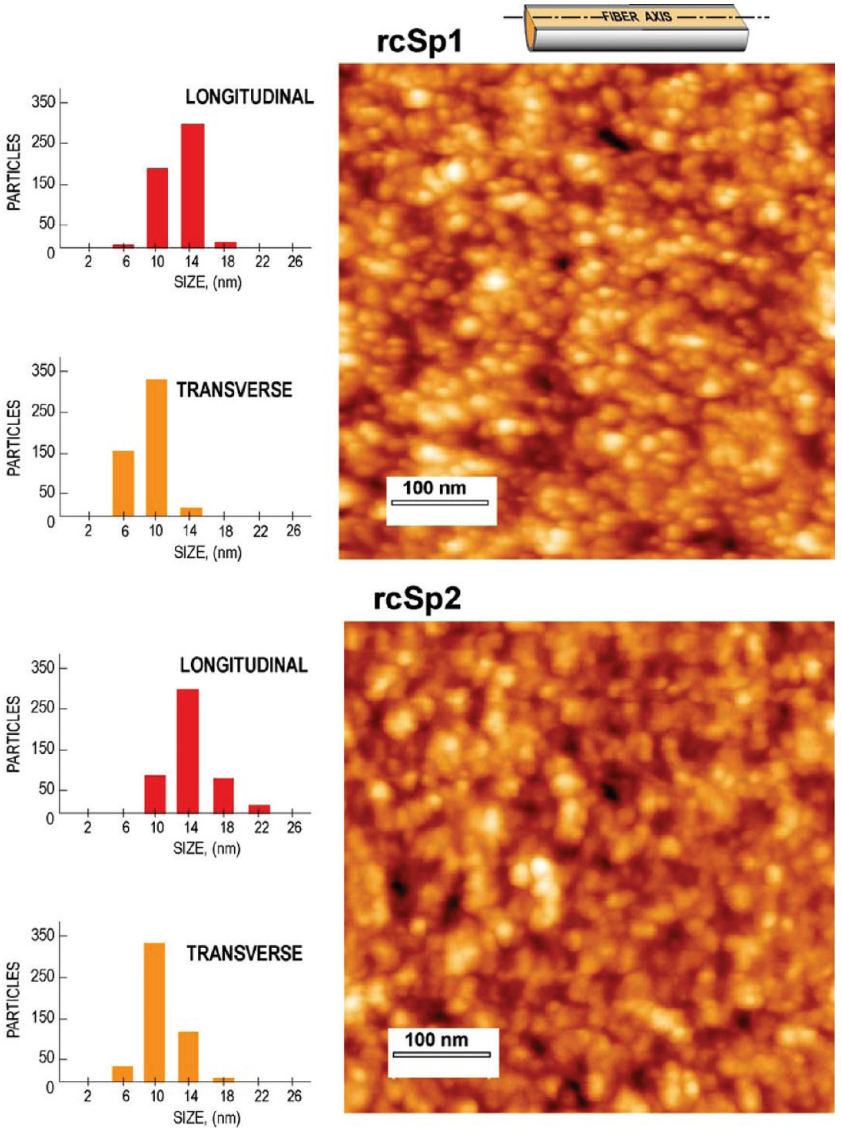

Figure 4. AFM micrographs of longitudinal sections of (a) pure rcSp1 (100%−0%) and (b) pure rcSp2 (0%−100%) fibers in the as spun condition. As illustrated in the inset, each micrograph is oriented so that the axis of the fiber lies on the horizontal direction. The histograms show the size of the nanoglobules, which are approximated by ellipses with a major and minor axis. For rcSp1, the mean value ± standard deviation is 13 ± 2 nm (major axis) and 10 ± 2 nm (minor axis), with a maximum size of 20 nm. For rcSp2, the sizes of the nanoglobules are 14 ± 3 and 11 ± 2 nm, with a maximum size of 27 nm.

1200 cm^{-1} contains bands characteristic of amino acid side chains (Figure 3c). The spectra appear similar but there are differences due to the different amino acid composition. Thus, rcSp2 spectrum shows additional bands at 875, 920, and 1042 cm^{-1} that correspond to proline,[57,58] an amino acid present in the sequence of rcSp2 but absent in the sequence of rcSp1 (Figure 1). No characteristic bands of the HFIP were identified from the Raman spectra, indicating that the solvent was eliminated during processing to a concentration below the detection limit of the technique. The region between 1100 and 1800 cm^{-1} (Figure 3d) contains the amide III band close to 1240 cm^{-1} and the amide I band near 1666 cm^{-1}, frequencies that are in agreement with a β-sheet conformation. The amide III mode involves mainly the stretching vibration of the C−N peptide bond, which is oriented in the β-sheet plane. The amide I mode consists mostly of the stretching vibration of the carboxyl C=O bond, which is oriented perpendicular to the β-sheet plane. Therefore, their polarization is very sensitive to the degree of orientation of the β-sheet crystallites.[30] For sheets perfectly aligned along the fiber axis z, the amide I band is stronger in the I_{xx} spectrum, whereas the amide III band is stronger in the I_{zz} spectrum. To compare quantitatively the degree of orientation the empirical parameter p defined by $p^2 = [I_{xx}(\mathrm{I}) \times I_{zz}(\mathrm{III})]/[I_{zz}(\mathrm{I}) \times I_{xx}(\mathrm{III})]$ has been used, where I and III refer to the amide I and amide III bands. This parameter cancels out any variations of intensity between I_{xx} and I_{zz} spectra due to focusing or equipment sensitivity and increases with the degree of orientation. In order to calculate p, spectra were fitted to a sum of Gaussian functions and a linear background in the 1100−1750 cm^{-1} range. Amide III intensity was taken as the total integrated area of Gaussians between 1215 and 1290 cm^{-1}. For amide I Gaussians between 1635 and 1720 cm^{-1} were added. For rcSp1 and rcSp2 values of $p^2 = 1.34$ and $p^2 = 1.02$ have been obtained that can be compared with the value of $p^2 = 1.1$ obtained from the Raman spectra of *Nephila edulis* MAS silk fibers,[42] indicating a higher degree of orientation for the rcSp1 protein.

6. Atomic Force Microscopy. The observation of longitudinal cuts of rcSp1 (100%−0%) and rcSp2 (0%−100%) fibers by atomic force microscopy reveals a homogeneous microstructure at a micrometer scale with no skin-core morphology, supporting the XRD data. Both samples show the usual nanoglobular microstructure at nanometer resolution found in natural[31] as well as in regenerated silk fibers,[59] as illustrated in Figure 4. The nanoglobules were approximated by ellipses and their major and minor axis measured. For rcSp1, the mean value ± standard deviation is 13 ± 2 nm (major axis) and 10 ± 2 nm (minor axis), with a maximum size of 20 nm. For rcSp2, the sizes of the nanoglobules are 14 ± 3 nm and 11 ± 2 nm, with a maximum size of 27 nm. The sizes of the nanoglobules are shown as histograms in the insets of Figure 4. The sizes of the nanoglobules are comparable to those found in natural silk fibers from the species *Argiope trifasciata*[31] (mean size of 13 ± 4 nm in forcibly silked fibers, and 10 ± 2 nm in maximum supercontracted fibers), and smaller than the sizes found in regenerated silkworm silk fibers.[31,42] The major axis of the nanoglobules appears to be more oriented with the macroscopic axis of the fiber in rcSp1 fiber than in the rcSp2. This preferential orientation along the macroscopic axis of the fiber might reflect the underlying long-range order revealed by the SAXS diffraction peak observed in the rcSp1 sample.

Final Discussion and Conclusions

How Close Are Recombinant Fibers to Natural Spider Silk? The results obtained provide important insight into what is needed and what is not, and which properties are easily reproduced and which are not in the search of high-performance artificial bioinspired fibers with the outstanding properties of major ampullate gland spider silk (MAS).

The synthetic fibers spun from dopes of recombinant silk proteins based on the spidroins of *Nephila* spiders through a wet spinning process reach values of the tensile parameters and, especially, of the work to fracture comparable to or even larger than those of high performance fibers, such as Kevlar 49, ultrahigh molecular weight polyethylene (UHMWPE)[16] or silkworm (*B. mori*) silk.[60] More significantly, the comparison of the stress−strain curves of bioinspired fibers with those of natural spider silk shows that both sets are essentially indistinguishable up to strains of 0.4. Besides, the concurrence of stress−strain curves is especially evident for the less ordered state of natural silk fibers, measured either through the ordered fraction (bioinspired fibers $f_{ord} \approx 0.3$) parameter[61,62] or through the alignment parameter (bioinspired fibers $\alpha \approx 0$).[40]

The similarity between bioinspired and natural silks suggests that the models used for the latter could also be applicable for the former. In this regard, the basic model of spider silk assumes a semicrystalline microstructure in which small nanocrystals are embedded in an essentially amorphous matrix. In terms of the interactions involved, the tensile behavior of spider silk is determined by a double network of hydrogen bonds established between spidroin proteins[63,64] and elastomeric chains.[39,65] Numerical models at a nanometer level indicate that spider silk is essentially composed of highly regular β-sheet nanocrystals arranged in a protein matrix of 3_1-helices and β-turn protein structures.[66] These models predict an initial elastic regime, which corresponds to the breaking of the hydrogen bonds in the matrix, followed by the unfolding of the secondary structures and, finally by the loading of the nanocrystals.[67] In this frame, the size of the nanocrystals in the range of ≈3 nm plays a critical role,[68] since it yields maximum toughness and allows the secondary structures of the matrix to unfold almost completely.[67] The tensile properties of bioinspired fibers fit in this model, indicating that the preservation of the size of the polyalanine runs as observed in the natural material might be a critical ingredient in the production of bioinspired fibers, since it ultimately determines the size of the nanocrystals. It also suggests that both the sequence and the processing route essentially preserve the organization of the amorphous matrix. Finally, it is also highlighted that there at least one further ingredient missing to explain the difference between natural and bioinspired fibers at very high deformations.

In the search for differences between natural and bioinspired fibers, it is evident that the molecular weight of recombinant proteins is approximately one-sixth of that of the natural spidroins. The results presented above indicate that the small molecular weight of the recombinant proteins (approximately 50 kDa) is not an obstacle to produce high performance fibers, but it does not clarify its influence at very high strains. Some reports indicate that the use of high molecular weight proteins may lead to a significant improvement of the tensile properties,[4] but the stress−strain curves shown differ essentially from those observed in the natural material.

Regarding the influence of the exact sequence of the spidroins, the availability of dopes with different compositions varying from pure rcSp1 to pure rcSp2 allowed analyzing the influence of the motifs in the performance of the fibers. Both rcSp1 and rcSp2 proteins contain the motif poly-A, which is considered to form crystalline regions of β-sheets.[69] The protein rcSp1 includes the motif GGX, and the protein

rcSp2 contains the motif GPGXX, where X is Tyr, Leu, or Gln. Both motifs have been implicated as elastic modules of the polymeric chains,[7,70] responsible of the high extensibility of the fibers.

It is notable that the rcSp1 and rcSp2 contain, in addition to the repetitive N-terminal domain, the highly conserved carboxyl(C)-terminal domain (nonrepetitive sequence), which shows high homology among various spider species (except for flagelliform silks[7]). This domain also contains a highly conserved cisteine residue, which is involved in interdisulfide cross-linking and pair to form dimers. Both the repetitive N-terminal and the C-terminal domains of spider silks have been implicated in the control of solubility and fiber formation. Assembly is supposed to be regulated by the charge distribution of the N-terminal which can be accelerated by a decrease in pH.[71,72] The C-terminal facilitates fiber formation by changes in ionic composition and/or mechanical stimuli, such as the shear stress applied for the formation of the fibers of the present study, known to align the repetitive sequence elements and promote β-sheet formation

Mechanical tests reveal that tensile properties exhibited in air are essentially the same for all the compositions—in particular for the two pure compositions—despite the different motifs that appear in the sequence. The similarity in the tensile properties demonstrates that the presence of proline is not necessary to yield elevated values of toughness, at least up to the values of tensile strength reached by recombinant fibers. This result is in agreement with models that compare the organization and tensile behavior of MaSp-1 (devoid of proline) and MaSp-2 (proline containing) proteins which found that, despite significant microstructural differences (see below), both proteins yield relatively similar mechanical behaviors.[68] However, proline motifs exert a clear effect on the tensile properties in water, increasing the compliance of the fibers, and in the microstructural parameters of the fibers in terms of crystalline fraction and orientation of the nanocrystals. These results are consistent with previous studies that proposed that the proline residues destabilize secondary structures and favor a more amorphous network structure[73] or even that the flexibility of the proteins in water is determined by the content of glycine and proline.[74]

Beside the good tensile properties discussed above, recombinant fibers show another salient feature: the existence of a ground state that can be reached by immersion in water. The ground state has usually been associated with the supercontraction of the fibers to the point that both terms are usually considered as synonyms. However, our results suggest revising this identification. Although recombinant fibers display all the effects customarily associated with supercontraction and the existence of a ground state—recovery from irreversible stretching, the possibility of modifying the properties predictably and reproducibly by stretching them and elastomeric behavior in water—the values of supercontraction are relatively modest varying from 16 to 24% after drying, far from the values of natural spider silk fibers.[45] Comparable values of contraction were found in synthetic fibers regenerated from *B. mori* fibroin solutions, which also show a ground state.[42] Consequently, we use the term supercontraction to refer to a dimensional change induced by water that allows reaching a ground state independently from the previous loading of the sample. In this sense, supercontraction does not presume a contraction larger than a given value, namely 20, 40, or 50%. This interpretation is consistent with the natural effect observed in spider silk fibers, since the value of the reduction in length depends on the initial state of the silk fibers (measured, for instance, by the alignment parameter). Consequently, the term supercontraction is assigned to the process independently from the initial state of the fiber. In addition these results prove that the presence of proline is not required for the fibers to show a ground state, as reported for major ampullate gland silk from nonorb web spinning spider species,[48] although it may play an effect in the quantitative extent of the process.[46]

The microstructural analysis shows that high-performance recombinant spidroin fibers share with natural MAS silk common microstructural features of alanine-rich crystalline domains embedded in a glycine-rich short-range order matrix.[50] In addition, a nanoscale organization is revealed by nanoglobular objects observed for recombinant and natural MAS silk by AFM (recombinant: 13−14 nm; MAS: 10−13 nm) and the presence of nanofibrillar objects by SAXS (rcSp1: ~7 nm periodicity). The comparison of the microstructural features observed by AFM and SAXS suggests the existence of weak electron density correlations in the bulk extending across several nanoglobules. In favorable cases, such as for natural *B. mori* silk (crystalline fraction ~60%), visual evidence for a nanofibrillar-type alignment of nanoglobular objects has been obtained by AFM,[31] although AFM is sensitive to the surface topography of the object rather than to bulk density modulations.

These similarities extend even to synthetic fibers regenerated from silkworm fibroin solutions[42] that yield values of 20% and 14−15 nm for the crystallinity and size of the nanoglobules, respectively. Since natural MAS, recombinant MAS and regenerated silkworm silk fibers show different compositions, these data highlight the importance of microstructure and suggest that the existence of a ground state and high performance tensile properties can be related to moderate values of crystallinity and to the presence of microstructural details in the range of 15 nm at the nanometer scale.

The main results of this work can be outlined as:

(1) It is possible to produce high performance bioinspired fibers indistinguishable from natural spider silk in terms of their tensile behavior except at very large deformations. Assuming that the properties in this range of deformations are essentially controlled by a combination of finely tuned nanocrystals and amorphous matrix,[75] these results indicate that this organization is significantly maintained in the bioinspired fibers. Major differences are still found at strains higher than 0.5 and, in particular, when the tensile strengths are compared.

(2) All the considered compositions yield fibers with similar tensile properties, except when tested in water. This similarity demonstrates that high toughness does not require the presence of proline, at least up to the values of tensile strength reached by recombinant fibers. However, the presence of proline is related with lower values of the orientation of the chains and of crystalline fraction, and is observed to increase the compliance of the fibers in water, consistently with previous studies on the flexibility of protein chains in water.[73,74]

(3) Recombinant fibers exhibit a ground state to which the fiber can revert regardless of its previous loading history. However, the values of supercontraction are relatively modest compared with those measured for natural spider silk fibers.[45] Besides, it is proven that the presence of proline is not required for bioinspired fibers to show a ground state.

These results indicate that high performance bioinspired fibers can be spun using conventional spinning technologies and a variety of compositions, whose tensile properties are essentially indistinguishable from those of the natural material up to large strains. These results imply that the initial prerequisites on the composition of the recombinant proteins can be significantly relaxed, while processing is appointed a leading role. The microstructural analysis indicates that a basic common organization characterized by a specific nanoglobular, low-crystallinity microstructure seems to underlie the excellent mechanical performance and properties of both bioinspired and natural silks. Finally, mimicking the tensile properties of natural properties at very large strains appears as the ultimate step in the production of spider silk-like bionspired fibers, and it could provide the last ingredient for our understanding of spider silk outstanding properties.

Acknowledgment. The authors would like to thank Dr. Andrew Rodenhiser for the production of the recombinant fibers. Ultramicrotomy was performed by E. Baldonedo (Centro de Microscopía Electrónica, Universidad Complutense de Madrid, Spain). Dr. A. Gil and L. Colchero (Nanotec Electrónica S.L., Madrid, Spain) offered support for the AFM observations. The authors are grateful to José Miguel Martínez for his help with the artwork. This work was funded by the Ministerio de Ciencia e Innovación (Spain) (Grant MAT 2009-10258), by Comunidad de Madrid (Grant MADR.IB-CM/S-SAL/0312/2006) and by Fundación Marcelino Botín.

Supporting Information Available: X-ray diffraction analysis of recombinant silk fibers. This material is available free of charge via the Internet at http://pubs.acs.org.

References and Notes

(1) Kaplan, D. L.; Lombardi, S.; Muller, W. S.; Fossey, S. A. *Biomaterials. Novel Materials from Biological Sources.*: Stockton Press: New York, 1991; p 53.
(2) Elices, M.; Perez-Rigueiro, J.; Plaza, G.; Guinea, G. V. *J. Appl. Polym. Sci.* **2004**, *6*, 3537–3541.
(3) Lewis, R. V. *Chem. Rev.* **2006**, *9*, 3762–3774.
(4) Xia, Q. Y.; Zhou, Z. Y.; Lu, C.; Cheng, D. J.; Dai, F. Y.; Li, B.; Zhao, P.; Zha, X. F.; Cheng, T. C.; Chai, C. L.; Pan, G. Q.; Xu, J. S.; Liu, C.; Lin, Y.; Qian, J. F.; Hou, Y.; Wu, Z. L.; Li, G. R.; Pan, M. H.; Li, C. F.; Shen, Y. H.; Lan, X. Q.; Yuan, L. W.; Li, T.; Xu, H. F.; Yang, G. W.; Wan, Y. J.; Zhu, Y.; Yu, M. D.; Shen, W. D.; Wu, D. Y.; Xiang, Z. H.; Yu, J.; Wang, J.; Li, R. Q.; Shi, J. P.; Li, H.; Li, G. Y.; Su, J. N.; Wang, X. L.; Li, G. Q.; Zhang, Z. J.; Wu, Q. F.; Li, J.; Zhang, Q. P.; Wei, N.; Xu, J. Z.; Sun, H. B.; Dong, L.; Liu, D. Y.; Zhao, S. L.; Zhao, X. L.; Meng, Q. S.; Lan, F. D.; Huang, X. G.; Li, Y. Z.; Fang, L.; Li, C. F.; Li, D. W.; Sun, Y. Q.; Zhang, Z. P.; Yang, Z.; Huang, Y. Q.; Xi, Y.; Qi, Q. H.; He, D. D.; Huang, H. Y.; Zhang, X. W.; Wang, Z. Q.; Li, W. J.; Cao, Y. Z.; Yu, Y. P.; Yu, H.; Li, J. H.; Ye, J. H.; Chen, H.; Zhou, Y.; Liu, B.; Wang, J.; Ye, J.; Ji, H.; Li, S. T.; Ni, P. X.; Zhang, J. G.; Zhang, Y.; Zheng, H. K.; Mao, B. Y.; Wang, W.; Ye, C.; Li, S. G.; Wang, J.; Wong, G. K. S.; Yang, H. M. *Science* **2004**, *5703*, 1937–1940.
(5) Ayoub, N. A.; Garb, J. E.; Tinghitella, R. M.; Collin, M. A.; Hayashi, C. Y. *PLoS ONE* **2007**, *6*, e514.
(6) Xu, M.; Lewis, R. V. *Proc. Natl. Acad. Sci. U.S.A.* **1990**, *18*, 7120–7124.
(7) Gatesy, J.; Hayashi, C.; Motriuk, D.; Woods, J.; Lewis, R. *Science* **2001**, *5513*, 2603–2605.
(8) Prince, J. T.; Mcgrath, K. P.; Digirolamo, C. M.; Kaplan, D. L. *Biochemistry (N.Y.)* **1995**, *34*, 10879–10885.
(9) Fahnestock, S. R.; Irwin, S. L. *Appl. Microbiol. Biotechnol.* **1997**, *1*, 23–32.
(10) Fahnestock, S. R.; Bedzyk, L. A. *Appl. Microbiol. Biotechnol.* **1997**, *1*, 33–39.
(11) Fukushima, Y. *Biopolymers* **1998**, *4*, 269–279.
(12) Scheller, J.; Guhrs, K. H.; Grosse, F.; Conrad, U. *Nat. Biotechnol.* **2001**, *6*, 573–577.
(13) Lazaris, A.; Arcidiacono, S.; Huang, Y.; Zhou, J. F.; Duguay, F.; Chretien, N.; Welsh, E. A.; Soares, J. W.; Karatzas, C. N. *Science* **2002**, *5554*, 472–476.
(14) Huemmerich, D.; Scheibel, T.; Vollrath, F.; Cohen, S.; Gat, U.; Ittah, S. *Curr. Biol.* **2004**, *22*, 2070–2074.
(15) Rammensee, S.; Slotta, U.; Scheibel, T.; Bausch, A. R. *Proc. Natl. Acad. Sci. U.S.A.* **2008**, *18*, 6590–6595.
(16) Chawla, K. K. *Fibrous Materials*; Cambridge University Press: Cambridge, U.K., 1998.
(17) Matsumoto, K.; Uejima, H.; Iwasaki, T.; Sano, Y.; Sumino, H. *J. Appl. Polym. Sci.* **1996**, *4*, 503–511.
(18) Um, I. C.; Ki, C. S.; Kweon, H. Y.; Lee, K. G.; Ihm, D. W.; Park, Y. H. *Int. J. Biol. Macromol.* **2004**, *1−2*, 107–119.
(19) Ha, S. W.; Tonelli, A. E.; Hudson, S. M. *Biomacromolecules* **2005**, *3*, 1722–1731.
(20) Marsano, E.; Corsini, P.; Arosio, C.; Boschi, A.; Mormino, M.; Freddi, G. *Int. J. Biol. Macromol.* **2005**, *4*, 179–188.
(21) Lock, R. L. Process for making silk fibroin fibers, Patent No. 5252285, **1993**.
(22) Hardy, J. G.; Romer, L. M.; Scheibel, T. R. *Polymer* **2008**, *20*, 4309–4327.
(23) Karatzas, C. N.; Chretien, N.; Duguay, F.; Bellemare, A.; Zhou, J. F.; Rodenhiser, A.; Islam, S. A.; Turcotte, C.; Huang, Y.; Lazaris, A. High-toughness spider silk fibers spun from soluble recombinant silk produced in mammalian cells. In *Biotechnology of Biopolymers*; Steinbüchel & Doi, Wiley-VCH: Weinheim, Germany, 2005; *Vol. 2*, pp 945−967.
(24) Perez-Rigueiro, J.; Viney, C.; Llorca, J.; Elices, M. *J. Appl. Polym. Sci.* **1998**, *12*, 2439–2447.
(25) Plaza, G. R.; Corsini, P.; Perez-Rigueiro, J.; Marsano, E.; Guinea, G. V.; Elices, M. *J. Appl. Polym. Sci.* **2008**, *3*, 1793–1801.
(26) Perez-Rigueiro, J.; Elices, M.; Guinea, G. V. *Polymer* **2003**, *13*, 3733–3736.
(27) Guinea, G. V.; Perez-Rigueiro, J.; Plaza, G. R.; Elices, M. *Biomacromolecules* **2006**, *7*, 2173–2177.
(28) Riekel, C.; Burghammer, R.; Davies, R.; Gebhardt, R.; Popov, D. Fundamentals of soft condensed matter scattering and diffraction with microfocus techniques. In *Applications of synchroton light to scattering and diffraction in materials and life sciences*; Ezquerra, T. A., Garcia-Gutierrez, M. C., Nogales, A. Gómez, M., Eds.; Springer Verlag: Heidelberg, Germany, 2008; pp 91−104.
(29) Hammersley, A. *FIT2D program*, in www.esrf.fr/computing/scientific/FIT2D/ **2009**.
(30) Rousseau, M. E.; Lefevre, T.; Beaulieu, L.; Asakura, T.; Pezolet, M. *Biomacromolecules* **2004**, *6*, 2247–2257.
(31) Perez-Rigueiro, J.; Elices, M.; Plaza, G. R.; Guinea, G. V. *Macromolecules* **2007**, *15*, 5360–5365.
(32) Garcia, R.; San Paulo, A. *Phys. Rev. B* **1999**, *7*, 4961–4967.
(33) Horcas, I.; Fernandez, R.; Gomez-Rodriguez, J. M.; Colchero, J.; Gomez-Herrero, J.; Baro, A. M. *Rev. Sci. Instrum.* **2007**, 1.
(34) Garrido, M. A.; Elices, M.; Viney, C.; Perez-Rigueiro, J. *Polymer* **2002**, *16*, 4495–4502.
(35) Work, R. W. *Text. Res. J.* **1977**, *10*, 650–662.
(36) Work, R. W.; Morosoff, N. *Text. Res. J.* **1982**, *5*, 349–356.
(37) Savage, K. N.; Guerette, P. A.; Gosline, J. M. *Biomacromolecules* **2004**, *3*, 675–679.
(38) Plaza, G. R.; Guinea, G. V.; Perez-Rigueiro, J.; Elices, M. *J. Polym. Sci., Part B: Polym. Phys.* **2006**, *6*, 994–999.
(39) Gosline, J. M.; Denny, M. W.; Demont, M. E. *Nature* **1984**, *5968*, 551–552.
(40) Guinea, G. V.; Elices, M.; Perez-Rigueiro, J.; Plaza, G. R. *J. Exp. Biol.* **2005**, *1*, 25–30.
(41) Liu, Y.; Shao, Z. Z.; Vollrath, F. *Nat. Mater.* **2005**, *12*, 901–905.
(42) Plaza, G. R.; Corsini, P.; Marsano, E.; Perez-Rigueiro, J.; Biancotto, L.; Elices, M.; Riekel, C.; Agullo-Rueda, F.; Gallardo, E.; Calleja, J. M.; Guinea, G. V. *Macromolecules* **2009**, *22*, 8977–8982.
(43) Fu, C. J.; Porter, D.; Shao, Z. Z. *Macromolecules* **2009**, *20*, 7877–7880.
(44) Perez-Rigueiro, J.; Viney, C.; Llorca, J.; Elices, M. *Polymer* **2000**, *23*, 8433–8439.
(45) Elices, M.; Plaza, G. R.; Arnedo, M. A.; Pérez-Rigueiro, J.; Torres, F. G.; Guinea, G. V. *Biomacromolecules* **2009**, *7*, 1904–1910.
(46) Liu, Y.; Sponner, A.; Porter, D.; Vollrath, F. *Biomacromolecules* **2008**, *1*, 116–121.
(47) Vollrath, F.; Porter, D. *Soft Matter* **2006**, *5*, 377–385.
(48) Pérez-Rigueiro, J.; Plaza, G. R.; Torres, F. G.; Hijar, A.; Hayashi, C.; Perea, G. B.; Elices, M.; Guinea, G. V. *Int. J. Biol. Macromol.* **2010**, 555–557.
(49) Bell, F. I.; McEwen, I. J.; Viney, C. *Nature* **2002**, *6876*, 37–37.

(50) Riekel, C.; Branden, C.; Craig, C.; Ferrero, C.; Heidelbach, F.; Muller, M. *Int. J. Biol. Macromol.* **1999**, *2*−*3*, 179–186.
(51) Marsh, R. E.; Corey, R. B.; Pauling, L. *Biochim. Biophys. Acta* **1955**, *1*, 1–34.
(52) Arnott, S.; Dover, S. D.; Elliott, A. *J. Mol. Biol.* **1967**, *1*, 201–208.
(53) Riekel, C.; Vollrath, F. *Int. J. Biol. Macromol.* **2001**, *3*, 203–210.
(54) Grubb, D. T.; Jelinski, L. W. *Macromolecules* **1997**, *10*, 2860–2867.
(55) Yang, Z.; Grubb, D. T.; Jelinski, L. W. *Macromolecules* **1997**, *26*, 8254–8261.
(56) Sapede, D.; Seydel, T.; Forsyth, V. T.; Koza, M. A.; Schweins, R.; Vollrath, F.; Riekel, C. *Macromolecules* **2005**, *20*, 8447–8453.
(57) Rousseau, M.; Lefevre, T.; Pezolet, M. *Biomacromolecules* **2009**, *10*, 2945–2953.
(58) Pellerin, C.; Rousseau, M. E.; Cote, M.; Pezolet, M. *Macromol. Symp.* **2005**, 85–98.
(59) Perez-Rigueiro, J.; Biancotto, L.; Corsini, P.; Marsano, E.; Elices, M.; Plaza, G. R.; Guinea, G. V. *Int. J. Biol. Macromol.* **2009**, *2*, 195–202.
(60) Perez-Riguero, J.; Elices, M.; Llorca, J.; Viney, C. *J. Appl. Polym. Sci.* **2001**, *9*, 2245–2251.
(61) Vollrath, F.; Porter, D. *Appl. Phys. A: Mater. Sci. Process.* **2006**, *2*, 205–212.
(62) Liu, Y.; Shao, Z. Z.; Vollrath, F. *Nat. Mater.* **2005**, *12*, 901–905.
(63) Termonia, Y. *Macromolecules* **1994**, *25*, 7378–7381.
(64) Termonia, Y. Molecular modelling of the stress/strain behaviour of spider dragline. In *Structural Biological Materials*; Elices, M., Ed.; Pergamon Press: Amsterdam, 2000; pp 335−349.
(65) Gosline, J. M.; Pollak, C. C.; Guerette, P. A.; Cheng, A.; Demont, M. E.; Denny, M. W. *Silk Polymers* **1994**, 328–341.
(66) Buehler, M. J. *Nano Today* **2010**, *5*, 379–383.
(67) Nova, A.; Keten, S.; Pugno, N. M.; Redaelli, A.; Buehler, M. J. *Nano Lett.* **2010**, *7*, 2626–2634.
(68) Keten, S.; Buehler, M. J. *J. R. Soc. Interface* **2010**, *53*, 1709–1721.
(69) Grubb, D. T.; Ji, G. D. *Int. J. Biol. Macromol.* **1999**, *2*−*3*, 203–210.
(70) Hinman, M. B.; Jones, J. A.; Lewis, R. V. *Trends Biotechnol.* **2000**, *9*, 374–379.
(71) Hagn, F.; Eisoldt, L.; Hardy, J. G.; Vendrely, C.; Coles, M.; Scheibel, T.; Kessler, H. *Nature* **2010**, 239–242.
(72) Askarieh, G.; Hedhammar, M.; Nordling, K.; Saenz, A.; Casals, C.; Rising, A.; Johansson, J.; Knight, S. D. *Nature* **2010**, 236–239.
(73) Savage, K. N.; Gosline, J. M. *J. Exp. Biol.* **2008**, *12*, 1937–1947.
(74) Rauscher, S.; Baud, S.; Miao, M.; Keeley, F. W.; Pomes, R. *Structure* **2006**, *11*, 1667–1676.
(75) Buehler, M. J. *Nature Nanotechnol.* **2010**, *3*, 172–174.